Boundary-Layer Meteorol (2008) 126:219–236
DOI 10.1007/s10546-007-9232-3

ORIGINAL PAPER

# Influence of Nocturnal Low-level Jets on Eddy-covariance Fluxes over a Tall Forest Canopy

**Thara V. Prabha · Monique Y. Leclerc · Anandakumar Karipot · David Y. Hollinger · Erich Mursch-Radlgruber**

Received: 26 April 2006 / Accepted: 11 September 2007 / Published online: 27 October 2007


**Abstract** Observations of low-level jets (LLJs) at the Howland AmeriFlux site in the USA and the jet's impact on nocturnal turbulent exchange and scalar fluxes over a tall forest canopy are discussed. Low-frequency motions and turbulent bursts characterize moderately strong LLJs, whereas low-frequency motions are suppressed during periods with strong LLJs and enhanced shear. An analysis based on the shear-sheltering hypothesis seeks to elucidate the effect of LLJs on flux measurements. In the absence of shear sheltering, large eddies penetrate the roughness sublayer causing enhanced mixing while during periods with shear sheltering, mixing is reduced. In the absence of the latter, 'upside-down' eddies are primarily responsible for the enhanced velocity variances, scalar and momentum fluxes. The integral length scales over the canopy are greater than the canopy height. The variance spectra and cospectra from the wavelet analysis indicate that large eddies (spatial scale greater than the low-level jet height) interact with active canopy-scale turbulence, contributing to counter-gradient scalar fluxes.

**Keywords** Carbon-dioxide flux · Countergradient fluxes · Eddy covariance · Low-level jet · Shear sheltering · Wavelet analysis

T. V. Prabha · M. Y. Leclerc (✉) · A. Karipot
Laboratory for Environmental Physics, The University of Georgia, 1109 Experiment Street, Griffin, GA 30223, USA
e-mail: Mleclerc@uga.edu

T. V. Prabha
Department of Biological and Agricultural Engineering, The University of Georgia, Griffin, GA, USA

D. Y. Hollinger
USDA Forest Service, Durham, NH, USA

E. Mursch-Radlgruber
Institute fuer Meteorologie und Physik (IMP-BOKU), Vienna, Austria

## 1 Introduction

Low-level jets (LLJs) are typical of the nocturnal stable boundary layer over land and are characterized by flow accelerations above the inversion layer (Blackadar 1957). Several studies (Beyrich 1994; Corsmeier et al. 1997; Kalthoff et al. 2000; Reitebuch et al. 2000) have linked the large-scale transport of water vapour and ozone and their nocturnal maxima to LLJ events. These features play a significant role in the nocturnal transport of momentum, mass, and energy by enhancing the turbulent exchange associated with shear production below the jet. In the presence of a low-level jet, vertical flux measurements in the stable boundary layer are influenced by an upside-down boundary layer characterizing turbulence detached from the surface (Mahrt 1999; Mahrt and Vikers 2002; Banta et al. 2006) due to the downward transfer of energy originating at and near the jet core (Banta et al. 2002). Depending on the proximity of the wind maximum to the surface, shear generation associated with LLJs can modify the exchange between the surface and the overlying atmosphere (Beyrich 1994; Banta et al. 2003), and can in several instances contribute to intermittent (Nappo 1991; Sun et al. 2002; Newsom and Banta 2002; Piper and Lundquist 2004) or continuous turbulence in the surface layer.

In the presence of a low-level jet, wind speed is increased not only at the jet height, but also in the lowest atmospheric layers as in the roughness sublayer (RSL). Over a tall canopy, the RSL is deeper than that over a rigid surface and coherent motions of the size of the canopy accomplish much of the turbulent exchange between the canopy and the atmosphere (Kaimal and Finnigan 1994). Active canopy-scale eddies and coherent motions arise from instabilities analogous to mixing-layer turbulence (Raupach et al. 1996), the growth rate of these instabilities depends on wind shear and contributes to larger amplitude instabilities during large-scale gusts. Canopy-scale motions contributing to the 'active' energy transfer generally become intermittent (Raupach et al. 1996) as the location and strength of the inflection in the velocity profile changes in the presence of gusty winds (Finnigan 1979). The increase in instabilities over the canopy may also lead to an amplification of canopy waves (Pulido and Chimonas 2001).

Turbulent bursts associated with LLJs and their role in modifying scalar fluxes over the canopy have not received much attention. During calm conditions, insufficient mixing results in the accumulation of $CO_2$ within the forest canopy. The buildup of $CO_2$ near the ground was found earlier to be coincident with high $CO_2$ flux events (Lee and Hu 2002) over complex terrain. The presence of a LLJ increases turbulent mixing within the RSL and flushes out $CO_2$ from the forest canopy (Karipot et al. 2006).

Hunt and Durbin (1999) discussed the influence of disturbances travelling at speeds significantly different from the free stream speed contributing to downbursts in the lower layers. They also explained situations where such external influences are sheltered from penetrating lower layers, a phenomenon sometimes found in the presence of a low-level jet with strong shear (Smedman et al. 2004). We explore evidence of shear sheltering (SS) in eddy-covariance data obtained over a forest canopy in the presence of a low-level jet. Disturbances that propagate from levels higher than the jet and their interaction with RSL are investigated.

The objective in this study is to investigate the role of LLJ and shear sheltering in modifying canopy-atmosphere momentum and scalar exchange above a 20 m tall forest canopy. We investigate how top-down eddies associated with LLJs play a role in modifying fluxes and how they affect spectral and cospectral characteristics. We also elucidate the role of shear sheltering on vertical momentum, heat and $CO_2$ exchange and identify scale-dependent characteristics over the canopy. We describe implications of LLJ-induced turbulence/blocking due to active turbulence/shear sheltering on carbon dioxide flux measurements.

## 2 Theory

Hunt and Durbin (1999) pointed out that, depending on the flow, 'two interacting velocity fields may mutually exclude each other across the interface' or 'resonate with each other producing increased turbulence at the interface'. In the mutually exclusive case, a strong shear layer may prevent eddies present at elevated layers from propagating down to the surface due to the shear-sheltering (SS) effect. Shear sheltering is a mechanism by which large eddies reaching the lower layers are suppressed by the presence of strong shear, resulting in the suppression of turbulence. This is in contrast with typical conditions where an increase in wind shear supports turbulence production. According to Hunt and Durbin (1999), an eddy moving toward a shear zone may induce vorticity in that zone. The formation of alternating areas of convergence and divergence in the shear zone introduces areas of upward motions to satisfy continuity, thus preventing the downward motion of the eddy. This can only happen when 'detached eddies moving with a horizontal speed close to that of the mean flow and having appropriate size are present above the wind maximum' (Hunt and Durbin 1999).

Smedman et al. (2004) proposed a criterion based on the shear-sheltering hypothesis to determine whether large eddies associated with the LLJ can penetrate lower atmospheric layers. They demonstrated that observations from two marine experimental sites in the Baltic Sea exhibited evidence of shear sheltering below the jet. A scaling parameter was defined, depending on the approximate vorticity variation across the shear layer given by $c = U_H/H^2$, where $U_H$ is the windspeed at the jet core and $H$ is the jet height. Cases with low $c$ values exhibit turbulence characteristics and velocity spectra typical of the atmospheric surface layer. When $c$ values are high, turbulence characteristics were those of a canonical boundary layer with a suppression of energy, indicating the effect of shear sheltering. The LLJ cases showed a suppression of energy compared to cases without a LLJ. Smedman et al. (2004) derived a non-dimensional parameter ($\Sigma_j$) from the curvature of the mean wind profile and the eddy scale given by:

$$\Sigma_j \approx \frac{(U_H/H^2)}{(dU/dz)^2 u_*^{-1}}, \tag{1}$$

where $u_*$ is the friction velocity and $dU/dz$ is the wind shear. The denominator of this equation represents a vorticity scale estimated from the horizontal length scale ($= u_*/(dU/dz)$).

Smedman et al. (2004) presented observational evidence that shear sheltering can occur over water bodies surrounded by land masses. Although low-level jets are common in the nocturnal boundary layer over land, evidence of such mechanisms and their effects on surface-atmosphere exchange are not recognized. Here we use the shear-sheltering hypothesis of Hunt and Durbin (1999) to establish a relationship between the characteristics of LLJs and eddy-covariance fluxes over a forest canopy. A sketch of the LLJ and shear layer under the influence of a tall canopy layer is presented in Fig. 1 following the concepts of Hunt and Durbin (1999) and Smedman et al. (2004), with particular application to our study. The amplitude of velocity fluctuations below the jet is considerably reduced due to the blocking effect associated with shear sheltering.

The investigation into how top-down eddies associated with a LLJ interact with the RSL and modify fluxes and the role of shear sheltering in preventing such effects, are of considerable importance in understanding nocturnal $CO_2$ exchange at sites where LLJs are commonly observed. An important question is whether these upside down eddies contribute to active, flux-contributing turbulence in the RSL where we seek an explanation using Townsend's hypothesis and its subsequent modification by McNaughton and Brunet (2002). Townsend's

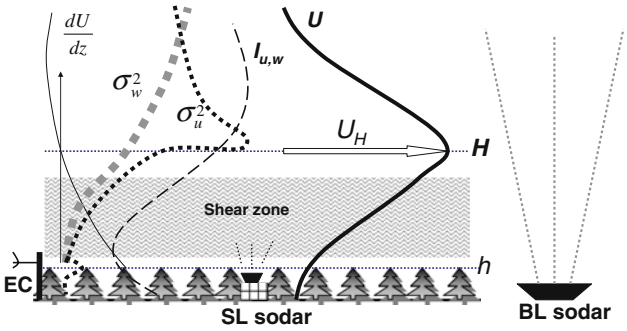


**Fig. 1** Schematic of the LLJ, shear zone and the experiment set-up (eddy covariance (EC) system, surface-layer (SL) sodar and boundary-layer (BL) sodar). Canopy height is indicated as '$h$'. $U$ is the wind speed profile (*thick line*), $dU/dz$ the wind shear (*thin line*), $\sigma_u^2$ the $u$ velocity variance (*thin dotted line*), $\sigma_w^2$ the $w$ velocity variance (*tick dotted line*) and $I$ the turbulence intensity (*dashed line*) (ratio of standard deviation of wind velocity and mean wind speed) are shown. $U_H$ is the wind speed at $H$ the jet height

hypothesis explains wall turbulence with an active part that transports momentum and an inactive part that does not. It is emphasized that the active and inactive parts do not interact with one another. McNaughton and Brunet (2002) have shown that the inactive component interacts with the active part in the convective boundary layer and, despite little impact on the momentum flux, scalar fluxes are affected. In cases where shear sheltering is weak, our study investigates whether Townsend's hypothesis is supported or whether it follows a behaviour described by McNaughton and Brunet (2002).

## 3 The Site Characteristics

The Howland AmeriFlux site (45.204°N, 68.740°W) is located on an approximately homogeneous terrain (Hollinger et al. 2004) with a coniferous forest canopy in the 80 km wide Penobscot River basin. The basin is situated in the lee side of the northern Appalachian mountain range, USA with elevations varying between 1 km and 2.9 km, with low mountains (≈300 m high) to the east. The site is located 100 km inland from the east coast (Gulf of Maine) with an elevation of 80 m above mean sea level. The forest canopy is 20 m tall. The topography within a 5 km region varies from flat to gently rolling, with small ridges and hills in the western and north-western sectors. The main ridge lies approximately 4 km away from the measurement location. LLJs in this region are possibly linked to baroclinic (possible influences from katabatic winds from the Appalachian mountain range) and sea-breeze frontal (due to the proximity to Atlantic Ocean) effects. LLJs are present in the Caribou to Portland (Bonner 1968) radiosonde data.

## 4 Experiment and Methods

Eddy-covariance (EC) measurements have been carried out at the Howland site since 1996 (Hollinger et al. 1999, 2004). A campaign involving boundary-layer sodar (PA2, Remtech Inc., France) and surface-layer sodar (Meteo Science, Vienna, Austria) measurements was conducted during the period 27 August – 7 September 2001. The surface-layer sodar was

mounted on a 12 m high platform in an opening in the forest at about 50 m distance from the AmeriFlux tower, and was used to measure three-dimensional velocities (at 0.5 Hz) up to a height of 100 m with a vertical resolution of 5 m. The boundary-layer sodar was located at a nearby clearing, 100 m away from the surface-layer sodar location and measurements extended up to a height of 1 km with a vertical resolution of 20 m. Figure 1 gives an outline of the measurement set-up.

The flux data are available from measurements made at a height of 29 m using a three-dimensional sonic anemometer (model SAT-211/3 K, Applied Technologies, Inc., Boulder, CO, USA) and a closed-path fast response $CO_2/H_2O$ infrared gas analyzer (model LI-6262, LiCor, Inc., Lincoln, NB, USA), with data sampled at 5 Hz. The measurement system and other signal processing details of the flux system are described in Hollinger et al. (1999). The time series of velocities, temperature and $CO_2$ concentration $x_n$ ($u$, $v$, $w$, $\theta$ and $CO_2$) sampled at 5 Hz subjected to co-ordinate rotation (Kaimal and Finnigan 1994) and detrending (Rannik and Vesala 1999) are used in the wavelet analysis. Each time series is normalized by the standard deviation of the respective parameter before being subjected to wavelet analysis.

Wavelet analysis (Daubechies 1991; Farge 1992; Meyers et al. 1993) is widely used to investigate coherent eddies of canopy turbulence (Collineau and Brunet 1993a, b; Gao and Li 1993; Turner et al. 1994; Qiu et al. 1995, Brunet and Irvine 2000). A continuous wavelet transform (Farge 1992; Daubechies 1993; Torrence and Compo 1998) has been used to study nocturnal turbulence and to isolate low-frequency events (Terradellas et al. 2001; Cuxart et al. 2002; Salmond 2005), described by:

$$W_n^x(s) = \sum_{n\prime=0}^{N-1} x_{n\prime} \Psi^* \left( \frac{(n\prime - n)\delta t}{s} \right). \tag{2}$$

A discrete set of 50 scales ($s$) of fractional powers of two is used. Scales are defined with $s_j = s_0 2^{j\delta j}$ with $j = 0, 1, \ldots J$, with $J = \log_2(N\delta t/s_0)/\delta j$, where $s_0 = 2\delta t$ is the smallest resolvable scale and $\delta j = 0.4$ gives a measure of scale resolution, $\delta t$ is the timestep and $\Psi^*$ is the transforming function representing the complex conjugate of the wavelet function $\Psi_0$, normalized with $\sqrt{\delta t/s}$ to ensure unit energy. The Morlet wavelet function (Grossman and Morlet, 1984) used in this study is given by $\Psi_0(t) = \pi^{-1/4} e^{i\omega_0 t} e^{-t^2/2}$, where the non-dimensional frequency $\omega_0 = 6$ and time t is non-dimensionalized. The approximate Fourier period corresponding to the oscillations within the Morlet wavelet is 1.03 times the scale; the hourly-averaged variance spectrum $W_n^x(s)^2$ is found from the square of the absolute value of wavelet power. The wavelet cross-spectrum (Katul and Parlange 1995; Terradellas et al. 2001; Cuxart et al. 2002) between the time series x ($u$, $\theta$ or $CO_2$) and vertical velocity ($w$) is given by:

$$CW_n^{w,x}(s) = s^{-2} W_n^w(s) W_n^{x*}(s). \tag{3}$$

The turbulent vertical exchange of $CO_2$ was partitioned into the co-gradient and counter-gradient flux contributions depending on the sign of the wavelet coefficients (Giostra et al. 2002; Cava et al. 2005) corresponding to $w$ and $CO_2$ concentration.

## 5 Results

LLJs were observed on all nights during the campaign with differing characteristics. Typically, before the initiation of the jet, south-westerly winds dominated the basin and were attributed to katabatic flow; several observed jets appeared to be initiated along with a shear

instability that propagated from higher levels. The EC measurements characterized several intermittent turbulent periods after the initiation of the LLJ, resembling bursts/microfronts (Prabha et al. 2007), though bursts were not observed on nights when the LLJ strength and wind shear below the jet increased beyond $0.02\,s^{-1}$. In low wind shear conditions, there is considerable variation in the three velocity components with the onset of the LLJ. Turbulent bursts were also present at a tower located 770 m west of the main tower with a 130 s delay on night 1, indicating a disturbance speed of $5.9\,m\,s^{-1}$. Similarly, on night 2, the disturbance propagated at $6.4\,m\,s^{-1}$. These propagation speeds are comparable to LLJ core wind speeds on nights 1 and 2.

Our analysis focuses on four nights where simultaneous EC and sodar data are available. General characteristics of the LLJs observed on four nights are given in Table 1. Moderate jets are observed on nights 1 and 2, while LLJs on nights 3 and 4 are strong and have a high vertical wind shear below 200 m. Cases chosen for the analysis are characterized by weakly stable to moderately stable conditions $(z - d)/L = 0.02$–$0.3$, where $z$ is the height above the surface, $d$ is the displacement height ($d = 0.68h$, where $h$ is the canopy height) and $L$ is the Obukhov length).

### 5.1 Application of the Shear-sheltering Hypothesis

To explore the role of shear-sheltering (SS) on burst events, $CO_2$concentration observations made in the lower part of the RSL are examined along with the SS parameter ($\Sigma_j$) in Fig. 2. $\Sigma_j$ is estimated (using Eq. 1 where $u_*$ is estimated at 29 m and $dU/dz$ is the vertical gradient of the mean wind speed $U$ is found between the jet height and 20 m above the ground) at every half-hour interval for four nights, focusing on data during the first half of each night for use in the analysis. Figure 2 shows that most periods characterized by low $CO_2$ concentration gradients (between 29 m and 5 m above the ground) correspond to lower values of $\Sigma_j$, suggesting an enhanced vertical mixing as a cause for the reduced concentration gradients. For higher values of $\Sigma_j$, large concentration gradients are possibly attributed to low mixing. The correlation coefficient between $\Sigma_j$ and the concentration gradient is 0.8, indicating the possibility that the turbulent mixing between the canopy airspace and the air above diminishes in shear-sheltering conditions and the accumulation of $CO_2$ within the canopy increases.

Figure 3 gives a comparison of wind speed, velocity standard deviations and wind shear ($dU/dz$) profiles derived from the sodar data for the cases classified according to the value of $\Sigma_j$. Data are averaged for 4 h, when the LLJ was fully developed and the 20 m wind speed is approximately half of the LLJ core (nose) wind. Data are also grouped into two classes characterized by either weak shear sheltering (low-SS) or strong shear sheltering (high-SS). It is noted that $\Sigma_j$ varies between 0.04 and 0.12 in the low-SS case and between 0.2 and 0.5 in the high-SS case; both cases correspond to weakly stable conditions with $(z - d)/L$ in the range 0.02–0.1. The low-SS case exhibits a lower wind speed and streamwise velocity standard deviation ($\sigma_u$) compared to the high-SS case. Both streamwise and vertical velocity standard deviations increased with height indicating that both cases have high turbulence above the LLJ core, possibly attributed to large-scale motions present above the LLJ. The vertical velocity standard deviation ($\sigma_w$) for both cases show similar values below 100 m, while a minimum in $\sigma_u$ and $\sigma_w$ can be seen at 200 m and 170 m in the low-SS and high-SS cases, respectively. These heights represent regions of minimum turbulence intensities as well ($\sigma_u/U$ and $\sigma_w/U$), indicating the existence of a less turbulent layer (Businger 1973) above which the flow accelerates. The flow accelerations lead to an increase in $\sigma_u$ and $\sigma_w$ corresponding to increased turbulence. A large positive shear is noted below 200 m in the

**Table 1** Comparison of LLJ characteristics on four nights

| | $U_H$(m s$^{-1}$) | H (m) | dU/dz_b (s$^{-1}$) | dU/dz_t (s$^{-1}$) | $U_{20\,m}$ (m s$^{-1}$) | Duration Onset-decay (hour) |
|---|---|---|---|---|---|---|
| Day 1 28 August 2001 | 7.5 (4.0–8.0) | 500 (440–500) | 0.01 | −0.01 | 2.5 (1.0–3.0) | 3 h and 15 min 1945–2300 |
| Day 2 29 August 2001 | 8.5 (5.5–14.0) | 280 (200–500) | 0.02 | −0.02 | 4.0 (2.0–6.0) | 12 h and 15 min 1845–0700 |
| Day 3 30 August 2001 | 11.5 (5.0–13.0) | 250 (220–450) | 0.04 | −0.02 | 5.2 (3.5–5.5) | 8 h 1900–0300 |
| Day 4 9 Sept. 2001 | 8.8 (6.0-15.0) | 490(350-620) | 0.03 | −0.01 | 4.5 (2.0–5) | 10 h and 30 min 1830–0400 |

$U_{20\,m}$ is the wind speed observed at 20 m, $H$ is the height of the jet, $U_H$ is the wind speed at the jet core, ($dU/dz\_b$) is the shear below the jet core (between the jet core and 20 m above ground) and ($dU/dz\_t$) is the shear above the jet core (between the jet core and 200 m above the jet core). Duration, onset and decay time of jets are also given. The values presented correspond to 2 h after the development of the LLJ and those in brackets are the range of values observed throughout the duration of the LLJ

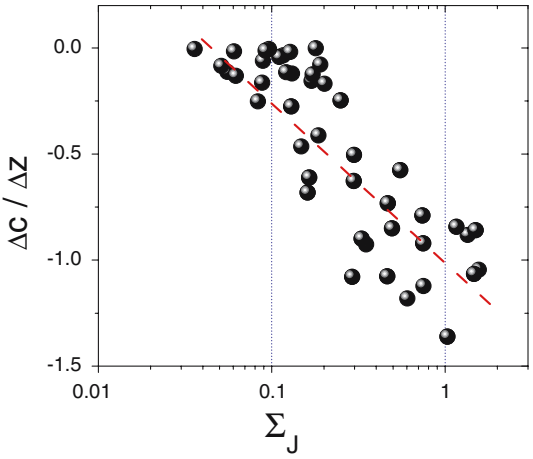


**Fig. 2** Variation of $CO_2$ concentration (ppm) gradient between 29 m and 5 m above the surface with shear-sheltering parameter ($\Sigma_j$)

high-SS case, while above the jet height $H$, the shear becomes negative. It is not significantly different between both cases.

The general behaviour that emerges from the cases classified according to the shear-sheltering parameter $\Sigma_j$ is the presence of a layer with minimum turbulence below the low-level jet. This layer is constantly eroded by the interaction of scales of motions that are comparable to or greater than $H$; the shear sheltering occurs only if motions that are comparable to $H$ are present above the LLJ core. Evidence for this is found in synoptic data indicating that large-scale motions were present above the LLJ on all four days analyzed.

### 5.2 Turbulence Characteristics over the Canopy

An examination of EC data at a height of 29 m shows signatures of downbursts during the low-SS case, while such features are absent in the high-SS case. Bursts introduce differences in the momentum exchange for two cases as shown by the probability density distributions (PDFs) of velocity fluctuations corresponding to low-SS and high-SS cases (Fig. 4a, b). The distribution of the momentum flux in each quadrant is also indicated in the figure. For the low-SS case (Fig. 4a), the momentum flux is dominated by strong sweeps ($u' > 0$, $w' < 0$, where the 'prime' is used to denote a deviation from hourly-averaged values) and weak ejections ($u' < 0$, $w' > 0$), resulting in a skewed $u'w'$ distribution similar to that of a PDF observed within the canopy (Raupach 1981; Shaw et al. 1983; Baldocchi and Meyers 1988). This behaviour suggests that sub-canopy momentum exchange is dynamically well-coupled with the atmosphere above. The large positive value (higher than 3.0) of the $u$ component kurtosis also indicates non-Gaussian turbulence in the low-SS case. The PDF of $u'w'$ is nearly Gaussian (Fig. 4b) in the high-SS case.

The low-SS case is characterized by high turbulence intensities ($\sigma_u/U$ in the range 0.4–1.0 and $\sigma_w/U$ in the range 0.2–0.4) in contrast with the high-SS case ($\sigma_u/U \approx 0.3$, $\sigma_w/U \approx 0.17$). The low-SS case also shows higher values ($> 1.5$) of normalized vertical fluxes of turbulent kinetic energy ($\overline{w'e}/u_*^3$, where e is the turbulent kinetic energy (TKE) given by $2e = \overline{u'^2} + \overline{v'^2} + \overline{w'^2}$) compared to the high-SS case. High TKE and the vertical flux of TKE at elevated layers, and an increase of shear production and dissipation rate (a tenfold

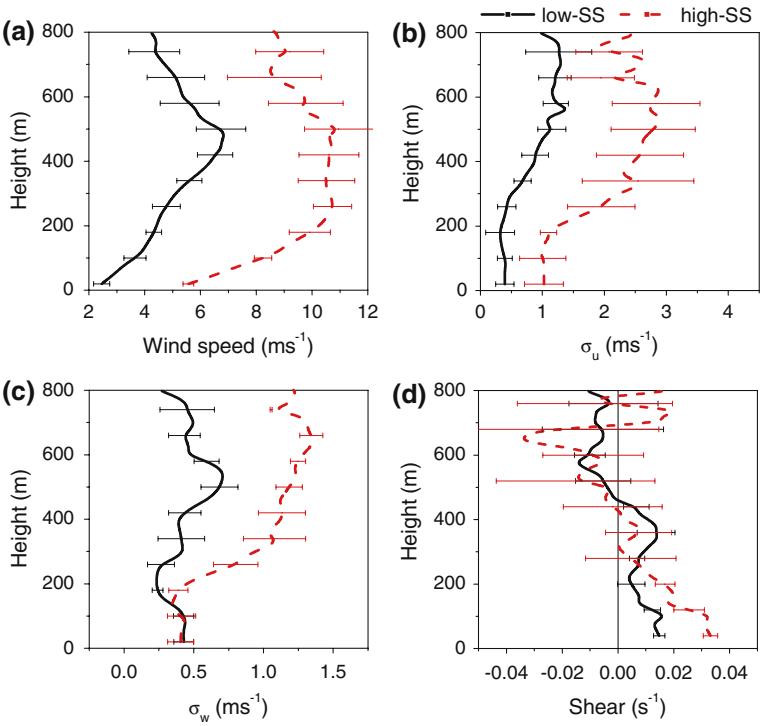


**Fig. 3** Vertical variation of (**a**) horizontal wind speed, (**b**) streamwise velocity standard deviation, (**c**) vertical velocity standard deviation and (**d**) wind shear observed with boundary-layer sodar in the presence of LLJs

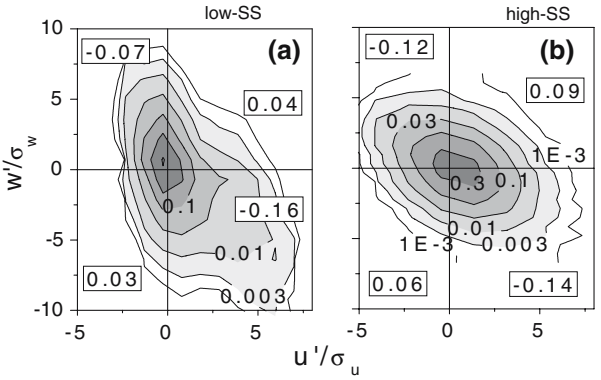


**Fig. 4** Probability distribution function of vertical velocity fluctuations with streamwise velocity fluctuations: (**a**) for low-SS case and (**b**) for high-SS case

increase beyond $z = 2.5h$ to $1\,\mathrm{m^2 s^{-3}}$ in the low-SS case compared to high-SS case) with height as evident from the TKE budget analysis (not presented) of the surface-layer sodar data, indicate the importance of pressure transport in the low-SS case. These results are in agreement with the concept that energy is transported away from the level of maximum production (Smedman et al. 1995).

In the low-SS case, the normalized streamwise velocity standard deviation ($\sigma_u/u_*$) is in the range 2–3.5, higher (1.9–2.1) than those observed in the high-SS case. The dimensionless streamwise velocity standard deviation ($\sigma_u(z)/u_*(z)$) from the surface-layer sodar in the height range of $1.7h$–$4h$ has a value between 2 and 3.4; we note a lower $\sigma_w/u_*$ during a high-SS case (0.5–1.0) compared to those in a low-SS case (0.7–1.5). Smedman et al. (2004) observed a decrease in $\sigma_w/u_*$ in the presence of shear sheltering. The vertical distribution of $\sigma_w$ inferred from sodar observations also shows similar results in the layers between $1.7h$ and $4h$. The normalized $\sigma_w(z)/u_*(z)$ from the surface-layer sodar is nearly constant with height between $1.7h$ and $3h$ for the high-SS case (1–1.2), in agreement with values reported near the canopy top ($\approx$1.0) and above ($\approx$1.25) by Finnigan (2000). For the low-SS case, $\sigma_w(z)/u_*(z)$ varies from 0.7 to 1.7 for the same vertical range and is inconsistent with Monin–Obukhov (MO) similarity calculations (Högström 1996). Högström (1990) found similar observational inconsistencies with MO similarity in the near-neutral atmospheric surface layer, which is attributed to active turbulence. A systematic increase in $\sigma_w/u_*$ with height ($\approx$1.0–2.1) at several sites (Högström et al. 2002) has been also linked to the presence of large eddies as explained by Hunt and Morrison (2000). Those observations corresponded to high Reynold numbers ($\approx 10^6$), which they attributed to detached large-scale eddies impinging on the surface.

The influence of shear sheltering on integral turbulent length scales at several levels above the canopy was also derived using the surface-layer sodar vertical velocity autocorrelation analysis. These results show lower values for the high-SS case ($<0.3h$ at heights between $1.7h$ and $3h$) while the low-SS length scales vary between $0.9h$ and $1.3h$. In the low-SS case, the length scale follows the relation $(z-d)/0.55$ just above the canopy as indicated by Kaimal and Finnigan (1994) for neutral stability, and increases rapidly in the surface-layer above $3h$. This is an indication that eddies scaling with canopy height or higher contribute to the vertical exchange in weak shear-sheltering conditions.

The low-SS case analyzed in this study is similar to that of Högström et al. (2002), where 'inactive' turbulence (Townsend 1961) interacts with 'active' turbulence over the canopy. It is yet to be determined whether these are indeed inactive motions or whether they contribute to shear stress and scalar flux. The scalar concentration variance and flux increase during the low-SS case compared to the high-SS case, and the half-hourly average standard deviation of the $CO_2$ concentration is higher in the low-SS case (2–4 ppm) compared to the high-SS case ($<$1 ppm). A large vertical exchange during weak shear sheltering contributes to high positive $CO_2$ flux (5–15 $\mu$mol m$^{-2}$s$^{-1}$) as opposed to the reduced flux (1–5 $\mu$mol m$^{-2}$s$^{-1}$) during a high-SS case. The $CO_2$ concentration also depicts a non-Gaussian behaviour, with a kurtosis greater than 3 in the low-SS case. The correlation coefficient between the temperature and $CO_2$ concentration decreases (0.75–0.4) considerably when large eddies penetrate deep into the RSL, while a high correlation (0.75–0.9) prevails when large eddies are shielded from penetrating to lower layers by a strong jet. This may be important when observations obtained in windy conditions are used in gap-filling algorithms of eddy fluxes in calm nocturnal conditions. A common procedure is to replace eddy fluxes during periods characterized by low friction velocities with fluxes derived from empirical relationships. Empirical relationships based on the respiration response to air, soil or bole temperature during windy conditions (Falge et al. 2001; Gu et al. 2005) are often used in gap-filling procedure. If observations during low-SS cases with lower correlation coefficient between the temperature and $CO_2$ concentration are used in the gap-filling procedure, resulting eddy fluxes may be erroneous.

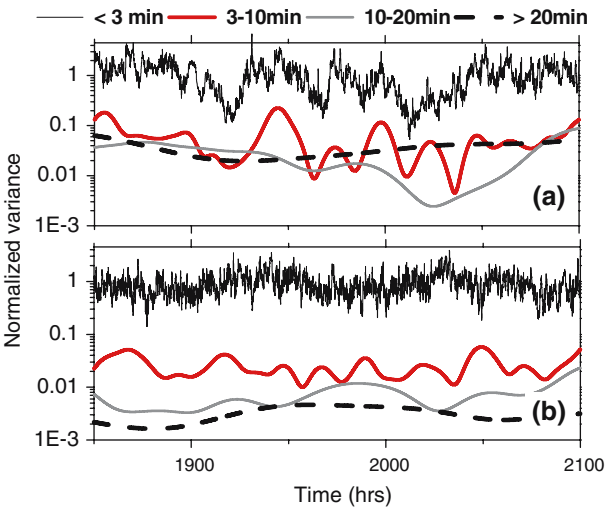


**Fig. 5** Multi-resolution decomposition of vertical velocity variance during (**a**) for low-SS and (**b**) for high-SS cases. Decomposition for Fourier periods less than 3 min (>0.0055 Hz), 3–10 min (0.0055–0.0017 Hz), 10–20 min (0.0017–0.00083 Hz) and greater than 20 min (<0.00083 Hz) are presented

### 5.3 Effects on Variance Spectra

The vertical velocity variance at different periodicities is obtained using a bandpass filtered inverse transform of wavelet coefficients (Terradellas et al. 2001). We considered two and a half hours long time series from both low-SS and high-SS cases to examine the contributions to vertical velocity variance from different eddy sizes. This period was chosen after examining the time series for low-frequency motions. The time variation of multi-resolution vertical velocity variance (Fig. 5) representing low-SS and high-SS cases is examined. Four denominations of Fourier period bands (<3 min, 3–10 min, 10–20 min, and >20 min) for corresponding frequencies are used to elucidate contributions from different periodicities. Data are normalized with corresponding hourly variances (total expected variance thus has a value of one). For the low-SS case, the low-frequency (higher period) variance is substantial compared to the high-SS case. There is a significant deviation around the variance value of one for Fourier periods less than 3 min (Fig. 5a) for the low-SS case, suggesting that the presence of large eddies also influences the energy associated with smaller eddies and thus high-frequency variances. However, such large deviations are replaced by small amplitude fluctuations in the high-SS case (Fig. 5b). The variance at periodicities below 3 min is modulated by variation in the periodicities between 3 min and 10 min in the low-SS case, while such effects are not evident in the high-SS case. These findings have consequences when short-term averages are used to eliminate the effects of low-frequency contributions to variances and fluxes.

The velocity and scalar spectra derived using the wavelet analysis are presented for low-SS and high-SS cases in Fig. 6, with spectra averaged over four hours (same period as in Fig. 3) of moderately stable conditions in both cases. The normalized spectral variance is plotted against the normalized frequency ($f(z-d)/U$, where $U$ is the hourly mean wind speed at $z = 29$ m). The $u$ and $v$ velocity spectra (Fig. 5a) during a low-SS case show a substantial enhancement of low-frequency contributions to variances not seen in the $w$ spec-

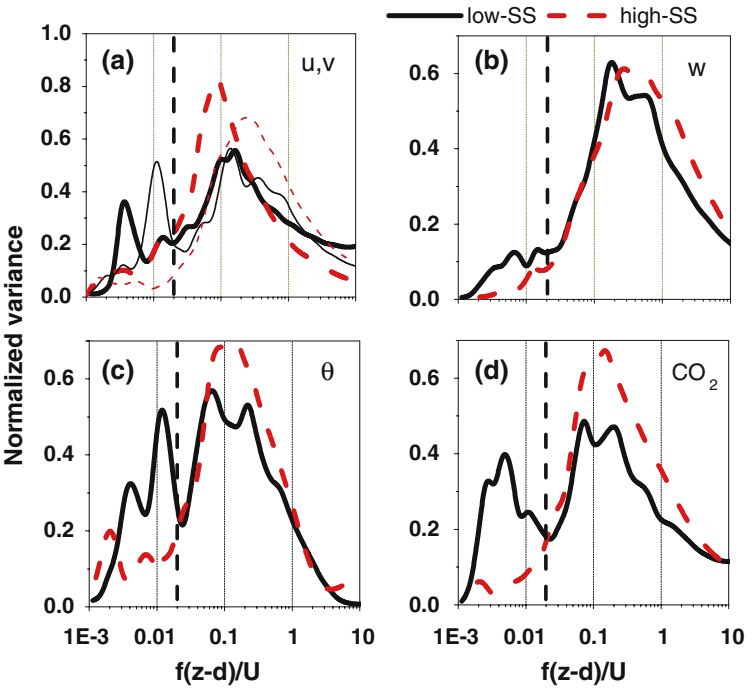


**Fig. 6** Average wavelet variance spectrum during low-SS and high-SS cases: (**a**) for $u$ (*thick lines*) and $v$ velocity (*thin lines*) components (**b**) for vertical velocity (**c**) for air temperature and (**d**) for $CO_2$ concentration. Spectra are normalized by respective variances and frequencies are normalized with wind speed ($(z-d)/U$, where $U$ is wind speed at $z = 29$ m and $d = 0.68h$). The *thick vertical dashed line* is used to indicate the separation between turbulent and large scales

trum (Fig. 5b). A spectral energy suppression is noted for all three velocity spectra at low frequencies for the high-SS case. In the low-SS case, a spectral gap (0.016–0.05) and a buoyancy subrange in the $v$ spectrum (0.011–0.019) are visible. They are less prominent in the $u$ spectrum (low-frequency peak is at 0.004). The peak energy for all three velocity variances is located between the normalized frequencies of 0.13 and 0.18. A lower separation between peaks indicates that energy-containing eddies are quasi three-dimensional in the low-SS case. Frequencies corresponding to $u$, $v$ and $w$ component peak variances during the high-SS case are more widely separated (0.08, 0.25, 0.27) than in the low-SS case. We separate the energy contribution to spectra into two regions; one with large eddies $f(z-d)/U < 0.02$ and the other with small eddies $f(z-d)/U > 0.02$ using the energy gap at 0.02. The percentage of $u$ variance in the low-SS and high-SS cases corresponding to large eddies (>H) is 42 and 15% in contrast with 58 and 85% for the smaller eddies.

The vertical velocity spectrum in the low-SS case shows a higher variance at lower frequencies (<0.035) than in the high-SS case, and indicates that large eddies contributed to vertical velocity variance in the low-SS case. A percentage estimate of the $w$ variance in the turbulence contribution to variance is 80% in the low-SS case while, in the high SS case, it is 99%. This indicates that 20% of the vertical velocity variance is contributed by large-scale motions. Spectra roll off with a $-2/3$ slope at higher frequencies for both cases if presented in a log-log representation. (Here a log-linear representation is used to highlight the importance of low-frequency contributions). In the low-SS case, there are two peaks in the $w$ spectra

located at normalized frequencies 0.164 and 0.007, while in the high-SS case, the single peak is located at 0.27. The approximate length scale of corresponding eddies are 93 m and 1.5 km for the low-SS case and 60 m for the high-SS case. These results indicate that larger-scale motions with length scales much higher than the LLJ height ($H$) also contribute to the $w$ variance in the low-SS case. The eddy size corresponding to the spectral peak at high frequency is approximately that of the depth of the layer (100 m) where velocity variances (Fig. 3b, c) are approximately constant. This layer also indicates the region of minimum turbulence intensity. The variance spectra of potential temperature (note the buoyancy subrange is the same as that of the $v$ spectra). The $CO_2$ concentration also shows that low-frequency contributions increase and high-frequency contributions decrease during the low-SS case (Fig. 6c, d).

### 5.4 Effect on Fluxes and Cospectra

The cospectra presented in Fig. 7 are normalized by the standard deviations of respective quantity pairs and thus represent the correlation coefficient between corresponding parameters. In order to demonstrate the effects of stability, we present the low-SS case data in two groups for four hours: one with moderately stable conditions ($(z-d)/L =$ 0.02–0.3, for the period used in the spectral analysis) and the other for near-neutral conditions ($(z-d)/L =$ 0–0.02). Higher low-frequency contributions to $uw$ (Fig. 7a), $w\theta$ (Fig. 7b) and $wc$ (Fig. 7c) correlations are evident in the absence of shear sheltering. The low-frequency contribution to the $r_{uw}$ value in the low-SS case (Fig. 7a) is attributed to the enhanced downward transfer of momentum giving rise to both intermittency and low-frequency transport. This is in contrast to the outer layer effects of convective boundary-layer transport where the momentum flux was not influenced, while scalar fluxes were (McNaughton and Brunet 2002). The correlation between scalars and vertical velocity ($r_{w\theta}$ and $r_{wc}$) during the low-SS case shows countergradient contributions at low frequencies. To investigate the cause of this low-frequency contribution to scalar flux, we analysed the phase difference ($\phi_{wx} = \tan^{-1}(Q/Co)$, where $Co$ is the wavelet cospectrum and $Q$ is the quadrature spectrum (Stull 1988) between the scalar and vertical velocity. The estimated phase difference is not representative of gravity waves (gravity waves show a phase shift of $\pm 90°$) but of turbulence. The intermediate frequency (0.036–0.32) correlations decrease with decreasing stability in the case of weak shear sheltering. It should be emphasized that corresponding wavelengths are 425–47 m and eddies of scales $\approx H$ take part in flux-contributing events. At a higher non-dimensional frequency (0.6) corresponding to the canopy height, we note another small peak for the low-SS case. This peak is well defined in the neutral case, indicative of the influence of low-SS on canopy-scale exchange. The cospectral peak for $r_{wc}$ (Fig. 7c) is present at the same frequency as that of the peaks in the $u$ variance and scalar variance spectra during the high-SS case, indicating the importance of streamwise transport.

To gain additional information on the multi-frequency exchange, we analyze the distribution of co-gradient and countergradient correlations (Giostra et al. 2002; Cava et al. 2005) separately for both low-SS and high-SS cases. The low-SS case shows a predominant countergradient correlation at low frequencies. The co-gradient correlations ($<0.027$) are also enhanced at lower frequencies. The co-gradient and countergradient contributions to fluxes in the high-SS case peak at 0.2. In the low-SS case, countergradient (0.2–0.31) and co-gradient (0.13–0.18) peaks are not located at the same frequencies in contrast to the high-SS case. This difference influences the location of the total correlation peak. If the co-gradient and countergradient correlation peaks are located at the same frequency, the total correlation decreases. The difference in peak locations results in sudden changes in the correlation as noted in the low-SS case. An examination of the flux contributing events at

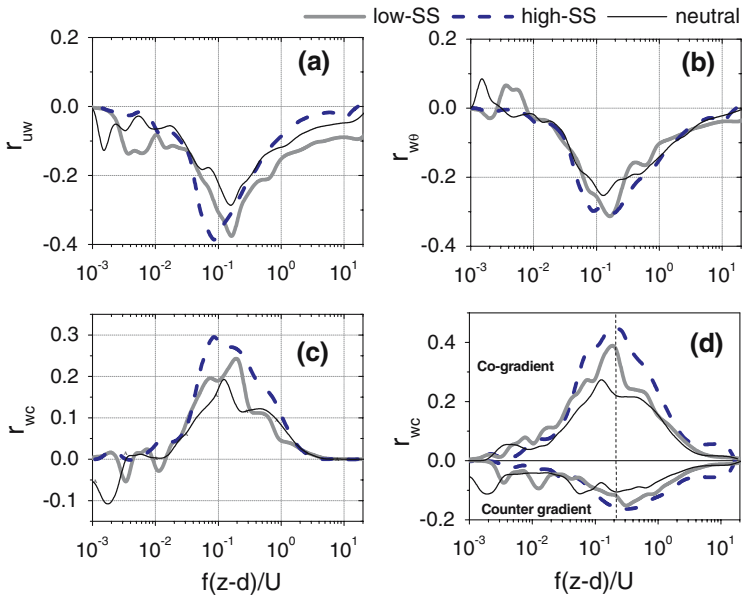


**Fig. 7** Wavelet spectra of correlation coefficient between (**a**) $u$ and $w$, (**b**) $w$ and $\theta$, and (**c**) $w$ and $CO_2$ concentration and (**d**) co-gradient and counter-gradient spectra of $w$ and $CO_2$ concentration

higher frequencies ($> 0.01$) shows that the number of events contributing to the negative flux is 5–10% more in the low-SS case. This suggests the presence of $CO_2$-rich sweeps and $CO_2$ depleted ejections at turbulence scales during the low-SS case. The countergradient contribution to fluxes at high frequencies is filtered out in the averaging process. However, there exists a large positive flux in the low-SS case influenced by low frequencies. We have noticed that the short period averaging (15 min) and trend removal gives large fluxes and the scatter in the resulting flux is also large. A longer averaging period yields lower resulting fluxes due to the presence of countergradient fluxes. In contrast, there is little countergradient flux for the high-SS case at lower frequencies and a short period averaging does not increase the flux.

The existence of distant terrain features (such as a mountain range) is often ignored while analyzing surface-layer and RSL turbulence. This may explain the origin of low-frequency events observed at this site. Low-frequency contributions to variances and countergradient fluxes in the presence of topographically induced disturbances have been reported by Smeets et al. (1998) in the Austrian Alps. In the present case, low-frequency motions are possibly caused by the presence of mountain waves interacting with the katabatic flow from the Appalachian mountain range. Poulos et al. (2000) demonstrate that the interaction between mountain waves and katabatic flow is complicated, with mutually evolving flow systems often indistinguishable from each other. The unsteady nature of these flow interactions is documented in small valleys (Mursch-Radlgruber 1995). Poulos et al. (2007) suggest that evolving and breaking mountain waves at elevated layers could introduce high-frequency oscillations in the surface layer. The present experimental findings observed during the low-SS cases agree with their results.

## 6 Conclusions

Nocturnal low-level jets were observed at the Howland AmeriFlux site on several nights. Their presence helps maintain turbulence and mixing in the roughness sublayer. Low-frequency events associated with moderate LLJs give rise to turbulent bursts in the RSL, contributing to active turbulence and mixing. However, low-frequency events are suppressed by the shear-sheltering (SS) effect (Smedman et al. 2004) in the presence of a strong jet with high wind shear and consequently turbulent mixing between the canopy airspace and the overlying air diminishes. The present results suggest that larger-scale motions with length scales much higher than the LLJ height contribute to the variances and fluxes when the shear-sheltering effect is weak. The penetration of large eddies during low shear-sheltering conditions also influences the energy associated with smaller eddies and thus high frequency contributions to variances and fluxes are also enhanced.

Significant countergradient contributions to scalar fluxes at low frequencies and enhanced co-gradient contributions both at low and high frequencies are noted during a low-SS case. In contrast, there is virtually no countergradient flux in a high-SS case at lower frequencies. A calm period followed by a more turbulent period is typical of burst events (Prabha et al. 2007) associated with the low-SS case, where a reduction in the flux at the initiation of the burst resulting from the countergradient contributions is followed by a large co-gradient flux attributed to the efflux of $CO_2$ from the canopy space. Observations of large effluxes of $CO_2$ from the canopy airspace (Hollinger et al. 2004) during turbulent events preceded by lower turbulence periods ($u_* < 0.2\,\mathrm{m\,s^{-1}}$) support these characteristics of the low-SS case. The intermittent and non-stationary behaviour during the low-SS case often induces high friction velocities, turbulence intensities and higher fluxes with considerable scatter. Such periods of observations in non-stationary conditions are often removed from the dataset leading to a bias towards lower fluxes with reduced ecosystem respiration (Wohlfahrt et al. 2005). The presence of countergradient fluxes also reduces the net flux and often goes unnoticed in a typical averaging period of 30 min. Our results suggest that observations of $CO_2$ during windy conditions associated with the presence of nocturnal low-level jets should be screened for the presence of such low-frequency effects.

**Acknowledgements** This work was supported by the Office of Science (BER), U.S. Department of Energy, through the Southeast Regional Center of the National Institute for Global Environmental Change. We thank the International Paper Company Ltd. for providing access to the research site in Howland, Maine. We also thank H. Hughes, J. Lee, and J. Walsh for their expert technical assistance. Findings and conclusions are the sole responsibility of the authors and do not necessarily represent the views of the DOE, NIGEC, or of International Paper Ltd. Three anonymous reviewers are thanked for their critical comments on the manuscript.

## References

Baldocchi DD, Meyers TP (1988) Turbulence structure in a deciduous forest. Boundary-Layer Meteorol 43:345–364

Banta RM, Newsom RK, Lundquist JK, Pichugina YL, Coulter RL, Mahrt L (2002) Nocturnal low-level jet characteristics over kansas during cases-99. Boundary-Layer Meteorol 105:221–252

Banta RM, Pichugina YL, Newsom RK (2003) Relationship between low-level jet properties and turbulence kinetic energy in the nocturnal stable boundary layer. J Atmos Sci 60:2549–2555

Banta RM, Pichugina YL, Alan BW (2006) Turbulent velocity-variance profiles in the stable boundary layer generated by a nocturnal low-level jet. J Atmos Sci 63:2700–2719

Beyrich F (1994) Sodar observations of the stable boundary-layer height in relation to the nocturnal low-level jet. Meteorol Zeitschrift 3:29–34

Blackadar AK (1957) Boundary layer wind maxima and their significance for the growth of nocturnal inversions. Bull Amer Meteorol Soc 38:283–290
Bonner WD (1968) Climatology of the low-level jet. Mon Wea Rev 96:833–850
Brunet Y, Irvine MR (2000) The control of coherent eddies in vegetation canopies: streamwise structure spacing, canopy shear scale and atmospheric stability. Boundary-Layer Meteorol 94:139–163
Businger JA (1973) Workshop on the planetary boundary layer. In: Haugen DA (ed) Amer Meteorol Soc 67–98
Cava D, Schipa S, Giostra U (2005) Investigation of low-frequency perturbations induced by a steep obstacle. Boundary-Layer Meteorol 115:27–45
Collineau S, Brunet Y (1993) Detection of turbulent coherent motions in a forest canopy, Part I: wavelet analysis. Boundary-Layer Meteorol 65:357–379
Collineau S, Brunet Y (1993) Detection of turbulent coherent motions in a forest canopy, Part II: timescales and conditional averages. Boundary-Layer Meteorol 66:49–73
Corsmeier U, Kalthoff N, Kolle O, Kotzian M, Fiedler F (1997) Ozone concentration jump in the stable nocturnal boundary-layer during a LLJ-event. Atmos Environ 31:1977–1989
Cuxart J, Morales G, Terradellas E, Yague C (2002) Study of coherent structures and estimation of the pressure transport terms for the nocturnal stable boundary layer. Boundary-Layer Meteorol 105:305–328
Daubechies I (1993) Ten Lectures on Wavelets. CBMS-NSF regional conference series in Applied Mathematics SIAM 61:357
Falge E, Baldocchi D, Olson R, Anthoni P, Aubinet M, Bernhofer C, Burba G, Ceulemans R, Clement R, Dolman H, Granier A, Gross P, Grünwald T, Hollinger D, Jensen N, Katul G, Keronen P, Kowalski A, Lai CT, Law BE, Meyers T, Moncrieff J, Moors E, Munger JW, Pilegaard K, Rannik Ü, Rebmann C, Suyker A, Tenhunen J, Tu K, Verma S, Vesala T, Wilson K, Wofsy S (2001) Gap filling strategies for defensible annual sums of net ecosystem exchange. Agric For Meteorol 107:43–69
Farge M (1992) Wavelet transforms and their applications to turbulence. Ann Rev Fluid Mech 24:395–457
Finnigan JJ (1979) Turbulence in waving wheat. I Mean statistics and Honami. Boundary-Layer Meteorol 16:181–211
Finnigan JJ (2000) Turbulence in plant canopies. Ann Rev Fluid Mech 32:519–571
Gao W, Li BL (1993) Wavelet analysis of coherent structures at the atmosphere–forest Interface. J Appl Meteorol 32:1717–1725
Giostra U, Cava D, Schipa S (2002) Structure functions in a wall-turbulent shear flow. Boundary-Layer Meteorol 103:337–359
Grossman A, Morlet J (1984) Decomposition of Hardy functions into square integrable wavelets of constant shape. SIAM J Math Anal 15:723–736
Gu LH, Falge EM, Boden T, Baldocchi DD, Black TA, Saleska SR, Suni T, Verma SB, Vesala T, Wofsy SC, Xu LK (2005) Objective threshold determination for nighttime eddy flux filtering. Agric For Meteorol 128:179–197
Högström U (1990) Analysis of turbulence structure in the surface layer with a modified similarity theory formulation for neutral conditions. J Atmos Sci 47:1949–1972
Högström U (1996) Review of some basic characteristics of the atmospheric surface layer. Boundary-Layer Meteorol 78:215–246
Högström U, Hunt JCR, Smedman A (2002) Theory and measurements for turbulence spectra and variances in the atmospheric neutral surface layer. Boundary-Layer Meteorol 103:101–124
Hollinger DY, Goltz SM, Davidson EA, Lee JT, TuK, Valentine HT (1999) Seasonal Patterns and environmental control of carbon dioxide and water vapour exchange in an ecotonal boreal forest. Global Change Biol 5:891–902
Hollinger DY, Aber J, Dail B, Davidson EA, Goltz SM, Hughes H, Leclerc MY, Lee JT, Richardson AD, Rodrigues C, Scott NA, Achuatavarier D, Walsh J (2004) Spatial and temporal variability in forest-atmosphere $CO_2$ exchange. Global Change Biol 10:1689–1706
Hunt JCR, Durbin PA (1999) Perturbed vortical layers and shear-sheltering. Fluid Dyn Res 24:375–404
Hunt JCR, Morrison JF (2000) Eddy structure in turbulent boundary layers. Euro J.Mech B – Fluids 19:673–694
Kaimal JC, Finnigan JJ (1994) Atmospheric boundary layer flows: their structure and measurement. Oxford University Press, UK, 304 pp
Kalthoff N, Horlacher V, Corsmeier U, Voltz-Thomas A, Kolahgar B, Giess H, Mollmann-Coers M, Knaps A (2000) Influence of valley winds on transport and dispersion of airborne pollutants in the Freiburg-Schauinsland Area. J Geophys Res 105:1585–1597
Karipot A, Leclerc MY, Zhang G, Martin T, Starr G, Hollinger D, Hipps LE, McCaughey LE, Anderson DJ, Hendrey GR (2006) Nocturnal $CO_2$ exchange over a tall forest canopy associated with intermittent low-level jet activity. Theor Appl Climatol 85:243–248

Katul GG, Parlange MB (1995) The spatial structure of turbulence in the dynamic and dynamic-convective sublayers using wavelet transforms. Boundary-Layer Meteorol 75:81–108
Lee X, Hu X (2002) Forest-air fluxes of carbon and energy over non-flat terrain. Boundary-Layer Meteorol 103:277–301
McNaughton KG, Brunet Y (2002) Townsend's hypothesis coherent structures and Monin-Obukhov similarity. Boundary-Layer Meteorol 102:161–175
Mahrt L (1999) Stratified atmospheric boundary layers. Boundary-Layer Meteorol 90:375–396
Mahrt L, Vickers D (2002) Contrasting vertical structures of nocturnal boundary-layers. Boundary-Layer Meteorol 105:351–363
Meyers SD, Kelley BG, O'Brien JJ (1993) An introduction to waveleta analysis in oceanography and meteorology: with application to the dispersion of Yanai waves. Mon Wea Rev 121:2858–28661
Mursch-Radlgruber E (1995) Observations of flow structure in a small forested valley system. Theor Appl Climatol 52:3–17
Nappo CJ (1991) Sporadic breakdown of stability in the PBL over simple and complex terrain. Boundary-Layer Meteorol 54:69–87
Newsom RK, Banta RM (2002) Shear-flow instability in the stable nocturnal boundary-layer as observed by Doppler lidar during CASES-99. J Atmos Sci 60:16–33
Piper M, Lundquist JK (2004) Surface layer turbulence measurements during a frontal passage. J Atmos Sci 61(14):1768–1780
Poulos GS, Bossert JE, McKee TB, Pielke RA (2000) The interaction of katabatic flow and mountain waves, Part I: observations and idealized simulations. J Atmos Sci 57:1919–1936
Poulos GS, Bossert JE, McKee TB, Pielke RA (2007) The interaction of katabatic flow and mountain waves. Part II: case study analysis and conceptual model. J Atmos Sci 64:1857–1879
Prabha TV, Leclerc MY, Karipot A, Hollinger DY (2007) Low-frequency effects on eddy covariance fluxes under the influence of a low-level jet. J Appl Meteor Climatol 46:338–352
Pulido M, Chimonas G (2001) Forest canopy waves: the long wavelength component. Boundary-layer Meteorol 100:209–224
Qiu J, Paw UKT, Shaw RH (1995) Pseudo-wavelet analysis of turbulence patterns in three vegetation layers. Boundary-layer Meteorol 72:177–204
Rannik U, Vesala T (1999) Autoregressive filtering versus linear detrending in estimation of fluxes by the eddy covariance method. Boundary-Layer Meteorol 91:259–280
Raupach MR (1981) Conditional statistics of reynolds stress in rough-wall and smooth-wall turbulent boundary layers. J Fluid Mech 108:63–382
Raupach MR, Finnigan JJ, Brunet Y (1996) Coherent eddies and turbulence in vegetation canopies. Boundary-Layer Meteorol 78:351–382
Reitebuch O, Strassburger A, Emeis S, Kuttler W (2000) Nocturnal secondary ozone concentration maxima analysed by sodar observations and surface measurements. Atmos Environ 34:4315–4329
Salmond J (2005) Wavelet analysis of intermittent turbulence in a very stable nocturnal boundary layer: implications for the vertical mixing of ozone. Boundary-Layer Meteorol 114:463–488
Shaw RH, Tavanger J, Ward DP (1983) Structure of the Reynolds stress in a canopy layer. J Climate Appl Meteorol 22:922–931
Smedman AS, Bergström H, Högström U (1995) Spectra variances and length scales in a marine stable boundary-layer dominated by a low-level jet. Boundary-Layer Meteorol 76:211–232
Smedman AS, Högström U, Hunt JCR (2004) Effects of shear-sheltering in a stable atmospheric boundary-layer with strong shear. Quart J Roy Meterol Soc 130:31–50
Smeets CJP, Duynkerke PG, Vugts HF (1998) Turbulence characteristics of the stable boundary layer over a mid-latitude glacier. Part I: C combination of katabatic and large-scale forcing. Boundary-Layer Meteorol 87:117–145
Stull RB (1988) An introduction to boundary layer meteorology. Kluwer Academic Publishers, Dordrecht, 666 pp
Sun J, Burns SP, Lenschow DH, Banta R, Newsom R, Coulter R, Frasier S, Ince T, Nappo C, Cuxart J, Blumen W, Lee X, Hu XZ (2002) Intermittent turbulence associated with a density current passage in the stable boundary-layer. Boundary-Layer Meteorol 105: 199–219
Terradellas E, Morales G, Cuxart J, Yagüe C (2001) Wavelet methods: application to the study of the stable atmospheric boundary-layer under non-stationary conditions. Dyn Atmos Oceans 34:225–244
Torrence C, Compo GP (1998) A practical guide to wavelet analysis. Bull Amer Meteorol Soc 79(1):61–78
Townsend AA (1961) Equilibrium layers and wall turbulence. J Fluid Mech 11:97–120
Turner BJ, Leclerc MY, Gauthier M, Moore KE, Fitzjaarald DR (1994) Identification of turbulence structures above a forest canopy using the wavelet transform. J Geophys Res 99D:1919–1926

Wohlfahrt G, Anfang C, Bahn M, Haslwanter A, Newesely C, Schmitt M, Drosler M, Pfadenhauer J, Cernusca A (2005) Quantifying nighttime ecosystem respiration of a meadow using eddy covariance, chambers and modelling. Agric For Meteorol 128:141–162